

Anisotropic Metamaterials for Full Control of Acoustic Waves

Johan Christensen¹ and F. Javier García de Abajo^{1,2,*}

¹*IQFR-CSIC Serrano 119, 28006 Madrid, Spain*

²*Optoelectronics Research Centre, University of Southampton, Southampton SO17 1BJ, United Kingdom*
(Received 10 October 2011; revised manuscript received 1 February 2012; published 23 March 2012)

We study a class of acoustic metamaterials formed by layers of perforated plates and producing negative refraction and backward propagation of sound. A slab of such material is shown to act as a perfect acoustic lens, yielding images with subwavelength resolution over large distances. Our study constitutes a nontrivial extension of similar concepts from optics to acoustics, capable of sustaining negative refraction over extended angular ranges, with potential application to enhanced imaging for medical and detection purposes, acoustofluidics, and sonochemistry.

DOI: 10.1103/PhysRevLett.108.124301

PACS numbers: 43.35.+d, 42.79.Dj, 81.05.Xj

Optical negative refraction is a counterintuitive phenomenon that consists in bending light the wrong way at the interface between suitably engineered materials. Homogeneous substances with refraction indices of opposite signs provide an ideal combination on which this effect can take place. Over four decades ago, Veselago [1] realized that a material with simultaneous negative magnetic permeability and electric permittivity must have negative index and, therefore, can produce negative refraction. Subsequently, Pendry [2] showed that a slab of such material can amplify evanescent fields, from which a perfect lens can be constructed, capable of yielding images with deep subwavelength resolution. These concepts have been realized in artificial metamaterials, textured on a small scale compared to the wavelength and displaying homogeneous resonant electric and magnetic response [3,4].

Inspired by these exotic optical phenomena, the quest for acoustic superlensing and negative refraction started with the prediction of negative index of refraction in materials exhibiting negative effective mass density and negative bulk modulus at the operating frequency [5]. In this context, several acoustic metamaterial designs have been proposed containing resonators in the form of coated metallic spheres [6], lumped elements [7], or perforations [8]. However, isotropic acoustic negative-index materials have not been experimentally realized to date, despite a long tradition of sound control using resonant linear devices [9,10], including applications to diffraction-limited imaging [11]. An alternative approach to acoustic negative refraction and lensing is suggested by electromagnetic metamaterials relying on anisotropy [12].

In this Letter, we show that a holey anisotropic metamaterial can exert subwavelength control over sound waves beyond what is achieved with naturally occurring materials. We predict that, for appropriate choices of geometrical parameters, these metamaterials support negative refraction, backward-wave propagation along a direction opposite with respect to the acoustic energy flow, and subwavelength imaging with both the source and the

image situated many wavelengths away from the material. Acoustic subwavelength control can be advantageous for (bio)medical ultrasonography and diagnostic imaging [13], acoustofluidic steering of microparticles and microorganisms [14], and sonochemistry enhanced by sound focusing [15,16].

We consider a bulk metamaterial design consisting of a stack of perforated plates made of an acoustically hard material (e.g., steel), separated by a sound-supporting fluid (e.g., air), as shown in Fig. 1(a), where all geometrical parameters are clearly defined. The elementary constituent is a 2D rigid hole array, the transmission properties of which have received considerable attention in connection to novel phenomena such as shielding of sound near the onset of diffraction [17], Fabry-Pérot resonances [18,19], and acoustoelastic resonances [20]. The pressure field ψ fully describes sound propagation in the fluid. We assume the holes to be small compared to both the sound wavelength λ and the lattice parameters, and we disregard elastic interactions in the hard screens. Under these conditions, it is safe to retain only the monopolar component of the field ψ^{scat} scattered by each hole in response to an incident pressure field ψ_0 . We can write

$$\psi^{\text{scat}}(\mathbf{r}) \approx \alpha \psi_0 \frac{e^{ik_0 r}}{r}, \quad (1)$$

where α is the scattering coefficient, $k_0 = 2\pi/\lambda$ is the sound wave vector, and the radial distance r is referred to the center of the aperture. Actually, we need to define scattering coefficients both for the near-side (reflection, α) and the far-side (transmission, α') scattering components of the hole. Inside the metamaterial, the *incident* field (from the hole point of view) originates in the scattered fields of the rest of the holes. In this way, one can write a set of self-consistent equations, which take a particularly simple form when the periodicity of the hole arrays is taken into consideration, so that we focus on a specific in-plane dependence of the pressure fields determined from Bloch's theorem via a parallel wave vector \mathbf{k}_{\parallel} : For holes facing a

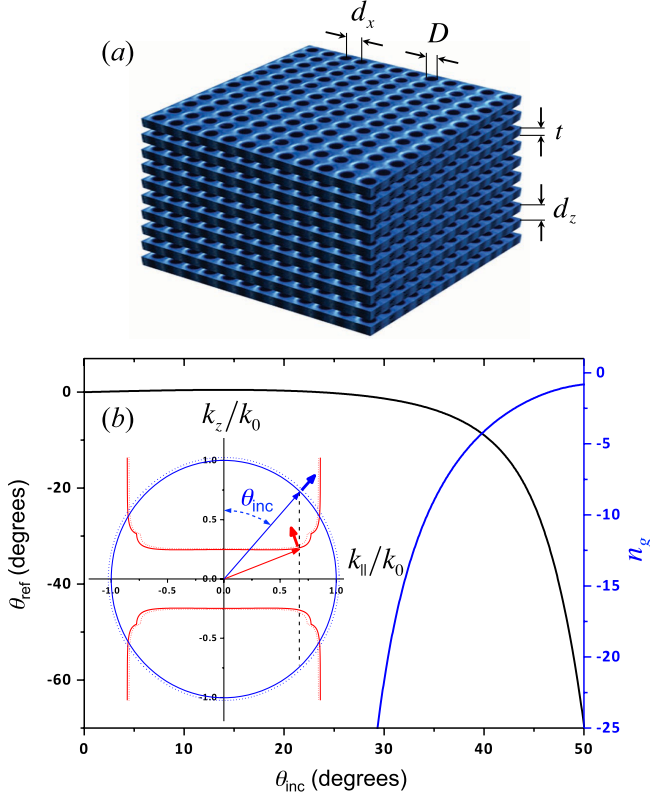


FIG. 1 (color online). (a) Schematic representation of an acoustic metamaterial consisting of stacked hard plates perforated by a periodic hole array. For simplicity, we consider a square array of period d_x and holes of diameter D . The plates of thickness t are separated by a distance $d_z - t$ (i.e., the period of the stack is d_z). The holes and the interstitial regions between the plates are filled with a sound-supporting medium in which the sound wavelength is λ . Perfect reflection of sound at the plate hard material is assumed. (b) Dependence of the refraction angle θ_{ref} and group refraction index n_g on incidence angle θ_{inc} for $d_z/d_x = 2.55$, $t/d_x = 1.9$, $D/d_x = 0.6$, and $\lambda/d_x = 1.95$ (this corresponds to 175 kHz in air for $d_x = 1$ mm). The inset shows equifrequency curves both in the homogeneous interstitial medium (circle of radius $k_0 = 2\pi/\lambda$) and in the metamaterial (hyperbolic dispersion curves) as a function of wave-vector components parallel and perpendicular to the plates, k_{\parallel} and k_z , respectively.

given fluid-filled interstitial gap region i , their incident pressure can then be written as $\beta_i \exp(i\mathbf{k}_{\parallel} \cdot \mathbf{R}_j)$, where \mathbf{R}_j are the in-plane position vectors of the hole-lattice sites j . In fact, the incident pressure can be different on the upper (β_i) and lower (β'_i) sides of each gap i . Putting these elements together, we derive the self-consistent equations

$$\begin{aligned}\beta'_i &= \alpha(G'\beta_i + G\beta'_i) + \alpha'(G'\beta'_{i-1} + G\beta_{i-1}), \\ \beta_{i-1} &= \alpha'(G'\beta_i + G\beta'_i) + \alpha(G'\beta'_{i-1} + G\beta_{i-1}),\end{aligned}$$

where G and G' are lattice sums extended over the holes of an interstitial region, together with their successive mirror

images at the surrounding plate planar boundaries. More precisely,

$$G = \sum_j \sum_{n=-\infty}^{\infty} \frac{\exp[ik_0 \sqrt{R_j^2 + 4n^2(d_z - t)^2}]}{\sqrt{R_j^2 + 4n^2(d_z - t)^2}} e^{ik_{\parallel} \cdot \mathbf{R}_j},$$

and G' takes a similar form with $4n^2$ substituted by $(2n+1)^2$. (Here, we need to eliminate from G the term with $\mathbf{R}_j = 0$ and $n = 0$, if it occurs.) A detailed derivation of these self-consistent relations is given in the Supplemental Material [21], in which we also provide comprehensive discussions on the numerical procedure followed to calculate the lattice sums.

The propagating modes of the metamaterial are determined by the condition $\beta_i = e^{\pm ik_z d_z} \beta_{i-1}$, where k_z is the wave vector along the perpendicular z direction. After some algebra, we find [21]

$$e^{\pm ik_z d_z} = \xi \pm \sqrt{\xi^2 - 1}, \quad (2)$$

where

$$\xi = \frac{1}{(g^- - g^+)G'} [(G - g^+)(G - g^-) - G'^2].$$

Now, in the absence of any losses, energy conservation for a single hole (incident energy = transmission + scattering) leads to the condition $\text{Im}\{g^{\pm}\} = -k_0$, where $g^{\pm} = 1/(\alpha - \alpha')$ [21]. Also, the lattice sums satisfy $\text{Im}\{G\} = -k_0$ and $\text{Im}\{G'\} = 0$ [21]. From these expressions, we conclude that ξ is real, and wave propagation is possible under the condition $|\xi| \leq 1$ with

$$k_z = (\pm 1/d_z) \cos^{-1} \xi. \quad (3)$$

The \pm sign in Eq. (3) is resolved by the physical condition $\text{Im}\{k_z\} > 0$, which guarantees nondivergent solutions $e^{ik_z z}$ for propagation towards increasing z (i.e., the direction of energy propagation). Then, backward-wave propagation occurs when $\text{Re}\{k_z\} < 0$ (i.e., the direction of energy propagation and the wave vector are opposite), which upon inspection of Eq. (2) is possible only if $\text{Im}\{\xi\} > 0$. In practical terms, we calculate the scattering coefficients α and α' analytically within the narrow-hole limit [21], and we add a small dissipation to these coefficients in order to determine the sign of $\text{Im}\{\xi\}$.

At this point, it is convenient to note that the group velocity $\mathbf{v}_g = \nabla_{\mathbf{k}} \omega$ describes the direction and speed of energy propagation inside the material. \mathbf{v}_g is normal to the equifrequency surfaces in wave-vector space, $\mathbf{k} = \mathbf{k}_{\parallel} + k_z \hat{\mathbf{z}}$. Since we have k_z expressed in terms of \mathbf{k}_{\parallel} and the frequency ω through Eq. (3), instead of ω in terms of \mathbf{k}_{\parallel} and k_z , we need to recast $\nabla_{\mathbf{k}} \omega$ into the equivalent expression $\mathbf{v}_g = (\partial k_z / \partial \omega)^{-1} (-\nabla_{\mathbf{k}_{\parallel}} k_z + \hat{\mathbf{z}})$. For $\mathbf{k}_{\parallel} = k_{\parallel} \hat{\mathbf{x}}$ along a high-symmetry direction $\hat{\mathbf{x}}$ of the planar hole arrays, we find $\nabla_{\mathbf{k}_{\parallel}} k_z = (\partial k_z / \partial k_{\parallel}) \hat{\mathbf{x}}$. It is also convenient to

define the group index of refraction n_g from Snell's law, which yields

$$n_g = -\frac{(k_{\parallel}/k_0)}{\partial k_z/\partial k_{\parallel}} \sqrt{1 + (\partial k_z/\partial k_{\parallel})^2}. \quad (4)$$

The value of k_{\parallel} is determined by the direction of the incident wave vector in the near side of the metamaterial. However, the group velocity inside the metamaterial can be directed along either the same (positive refraction) or the opposite direction (negative refraction), depending on whether the sign of $\partial k_z/\partial k_{\parallel}$ is negative or positive, respectively. Thus, positive (negative) refraction corresponds to $\text{Re}\{n_g\} > 0$ ($\text{Re}\{n_g\} < 0$), according to Eq. (4).

Next, we show that these holey metamaterials exhibit broad-angle negative refraction, unlike fishnet electromagnetic metamaterials, which operate within narrow angular ranges [4]. The proposed metamaterials do not rely on diffraction to achieve negative refraction, in contrast to phononic crystals [22]. The inset in Fig. 1(b) shows equifrequency curves for the wave vector of propagating modes in air (circle) and in a representative metamaterial (red curves) with a hole spacing of 1 mm, operating at a frequency of 175 kHz (see the caption for additional parameters). The incident wave vector (radial in air) is shown for an angle of incidence $\theta_{\text{inc}} = 42^\circ$. Transmission across the interface must preserve the parallel wave vector, and this determines the transmitted direction inside the metamaterial. Now, the group velocity is normal to the equifrequency contours and oriented towards the direction of increasing frequency [dotted equifrequency curves are shown in the inset in Fig. 1(b) for a frequency slightly above 175 kHz]. In our example, the propagation direction is oriented to the right in air (blue arrow) and towards the left once inside the metamaterial (red arrow), thus indicating that negative refraction occurs at this interface. We confirm this behavior by numerically calculating the refraction angle θ_{ref} displayed by a refracted Gaussian beam (see Fig. 2), in full agreement with Snell's law [$\sin\theta_{\text{inc}} = n_g \sin\theta_{\text{ref}}$; see Eq. (4)]. The main part of Fig. 1(b) shows both the refraction angle (left scale) and the group index of refraction (right scale) as a function of incidence angle, demonstrating a broad angular range over which negative refraction takes place. From the above construction, this is clearly a consequence of the hyperbolic dispersion shown in the inset.

We now focus on the refraction of a Gaussian beam passing through a metamaterial slab. The beam is constructed as a sum of $\sim 10^3$ plane-wave components. Specifically, we investigate the spatial evolution of the field as it traverses the interfaces between air and the metamaterial for the same geometrical parameters as in Fig. 1 but truncating the crystal to 250 layers. We apply a closed-form expression for the transmission and reflection coefficients [21], resulting from a recursion that allows us to propagate \mathbf{k}_{\parallel} -dependent waves between successive

layers. Figure 2 shows the resulting simulations for incidence with an angle of 42° on the left surface of the slab. We observe negative refraction at a frequency of 175 kHz [Fig. 2(a); the power transmittance is 70%], associated with forward waves on both sides of the interface [Fig. 2(b)] and originating in the hyperbolic dispersion noted above [Fig. 1(b), inset]. In contrast, positive refraction occurs at 95 kHz [Fig. 2(c)], accompanied by a backward wave in the metamaterial [Fig. 2(d)].

Given the broad degree of control over refraction and propagation of airborne sound displayed by these holey structures, we next explore the possibility of using a metamaterial slab as a lens. Imaging of subwavelength sources has been proposed with devices such as endoscopes [8], negative-refraction perfect lenses [2], and slabs supporting slow modes [23]. Subwavelength imaging relies on the reconstruction of tiny details of the object via amplification of evanescent waves. Metamaterial slabs can be engineered to precisely do that, as we show in Fig. 3 for a metamaterial operating at a frequency of 62 kHz, which is capable of imaging a point source located $\approx 30\lambda$ away from the metamaterial lens. The slab is made up of 50 layers. First, we observe a tight focus inside the slab close to the near-side interface. But more importantly, at a distance of $\approx 18\lambda$ away from the far side of the lens (i.e., ≈ 0.6 times the slab thickness), an image spot is observed with a lateral FWHM 5 times smaller than the wavelength (see the inset). This confirms the capability of holey metamaterials to operate as lenses with subdiffraction-limit resolution for relatively large distances between the source or image and the lens. Interestingly, the spectral dependence of the FWHM of the image spot [Fig. 3(b)] shows a dip near a

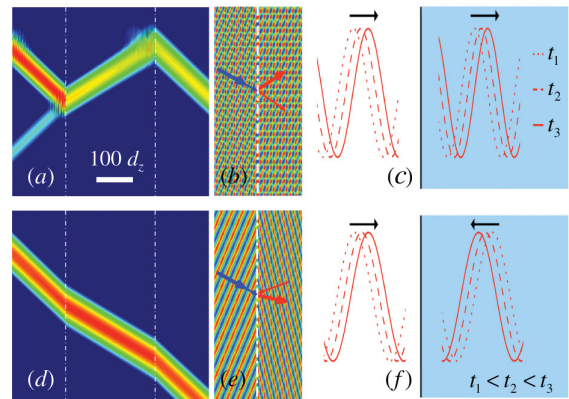


FIG. 2 (color online). Pressure-field simulations for a finite metamaterial containing 250 layers with the same geometrical parameters as in Fig. 1. (a) Negative refraction for a Gaussian beam incident with angle $\theta_{\text{inc}} = 42^\circ$ from the left with wavelength $\lambda = 1.95d_x$ (175 kHz in air for $d_x = 1$ mm.). Broken lines indicate the slab interfaces. (b),(c) Phase (b) and group (c) front propagation are both along the incidence direction in this case. (d) The same as (a) for $\lambda = 3.56d_x$ (95 kHz in air for $d_x = 1$ mm.), giving rise to positive refraction. (e),(f) Backward-wave propagation is observed at this new wavelength.

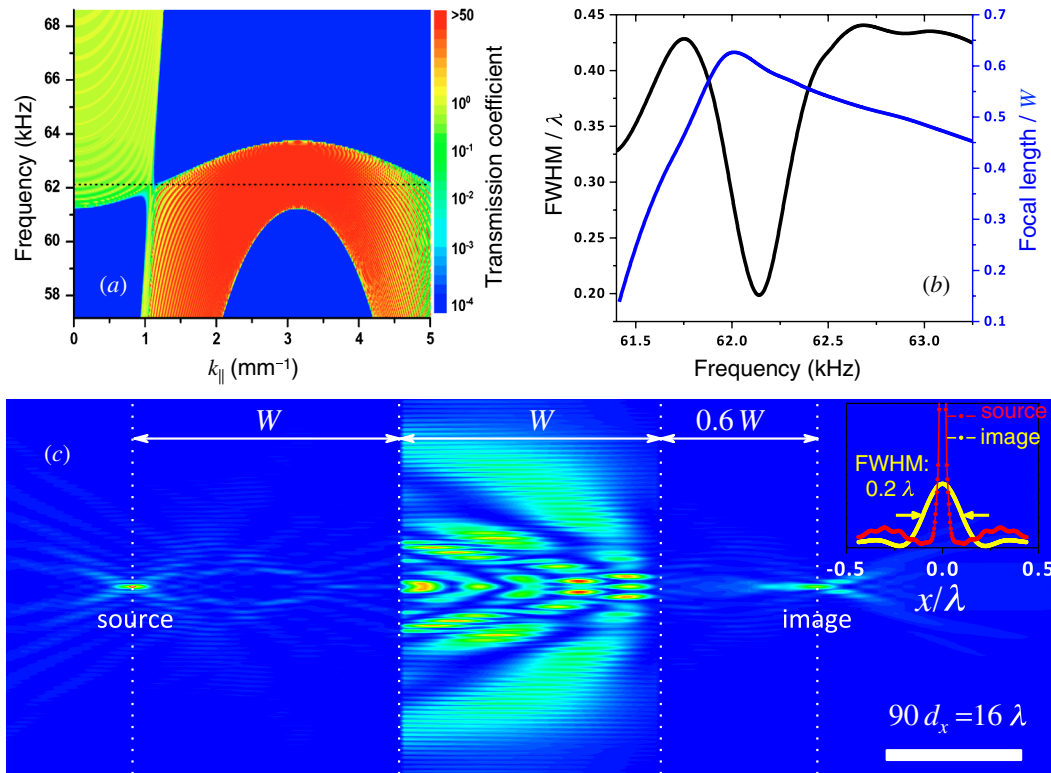


FIG. 3 (color online). Evidence of sound focusing in the calculated pressure-field distribution for an anisotropic metamaterial slab. (a) Frequency and parallel wave-vector dependence of the transmittance through a metamaterial slab consisting of 50 steel plates immersed in air with parameters $t/d_x = 2.5$, $d_z/d_x = 3.5$, $D/d_x = 0.6$, and $d_x = 1$ mm. The transmittance is defined as the squared amplitude of the far-side zero-order wave upon irradiation with a wave of unit amplitude at the near-side interface. (b) Focal length from the far side of the slab to the image (right) and FWHM of the image spot (left) as a function of sound frequency. The source is placed at a distance from the slab equal to the slab thickness W in all cases. (c) Near-field intensity distribution showing the image at a distance $\sim 0.6 W$ from the far side of the slab for a frequency of 62 kHz, which corresponds to $\lambda/d_x = 5.52$. The inset illustrates the transversal intensity profiles around the source (a pointlike monopole) and the image (FWHM $\approx 0.2\lambda$).

frequency of 62 kHz, for which evanescent waves have large transmittance [Fig. 3(a)]; this further emphasizes the role of evanescent waves as carriers of subwavelength details for the reconstruction of a tight image spot. High transmission in the present case occurs due to nonresonant coupling to guided modes of the metamaterial. Finally, it should be noted that this lens is robust against absorption for a realistic choice of materials [21].

In conclusion, we have demonstrated that holey anisotropic metamaterials produce a vast range of unusual behavior, encompassing negative refraction and backward-wave propagation. In particular, negative refraction is achieved over a broad range of incidence angles. We have also explored the focusing properties of metamaterial slabs, which can produce subdiffraction-limited imaging at distances of several wavelengths from the slab boundaries. In a practical application, the image spot could be scanned over the interior of a sampled body and an image constructed out of the resulting scattering signal (e.g., for medical imaging). Our illustrative calculations are made for ultrasound frequencies in ranges of operation that are common in ultrasonography and general biomedical

applications, for which these metamaterials provide a versatile fabric.

This work has been supported by the Spanish MICINN (MAT2010-14885 and Consolider NanoLight.es) and the European Commission (FP7-ICT-2009-4-248909-LIMA and FP7-ICT-2009-4-248855-N4E). J.C. gratefully acknowledges financial support from The Danish Council for Independent Research (Natural Sciences) under Contract Metacoustics 2011 10-093234. F.J.G.A. acknowledges support from the Leverhulme Trust.

*Corresponding author.

J.G.deAbajo@csic.es

- [1] V. G. Veselago, *Sov. Phys. Usp.* **10**, 509 (1968).
- [2] J. B. Pendry, *Phys. Rev. Lett.* **85**, 3966 (2000).
- [3] J. B. Pendry, A. J. Holden, D. J. Robbins, and W. J. Stewart, *IEEE Trans. Microwave Theory Tech.* **47**, 2075 (1999).
- [4] J. Valentine, S. Zhang, T. Zentgraf, E. Ulin-Avila, D. A. Genov, G. Bartal, and X. Zhang, *Nature (London)* **455**, 376 (2008).
- [5] J. Li and C. T. Chan, *Phys. Rev. E* **70**, 055602(R) (2004).

- [6] Z. Y. Liu, X. X. Zhang, Y. W. Mao, Y. Y. Zhu, Z. Y. Yang, C. T. Chan, and P. Sheng, *Science* **289**, 1734 (2000).
- [7] N. Fang, D. Xi, J. Xu, M. Ambati, W. Srituravanich, and X. Zhang, *Nature Mater.* **5**, 452 (2006).
- [8] J. Zhu, J. Christensen, J. Jung, L. Martín-Moreno, X. Yin, L. Fok, X. Zhang, and F. J. García-Vidal, *Nature Phys.* **7**, 52 (2011).
- [9] G. W. Stewart, *Phys. Rev.* **20**, 528 (1922).
- [10] S. H. Lee, C. M. Park, Y. M. Seo, Z. G. Wang, and C. K. Kim, *Phys. Rev. Lett.* **104**, 054301 (2010).
- [11] S. Zhang, L. Yin, and N. Fang, *Phys. Rev. Lett.* **102**, 194301 (2009).
- [12] D. R. Smith and D. Schurig, *Phys. Rev. Lett.* **90**, 077405 (2003).
- [13] M. Sackmann, M. Delius, T. Sauerbrucht, J. Holl, W. Weber, E. Ippish, U. Hagelauer, O. Wess, W. Hepp, W. Brendel, and G. Paumgartner, *N. Engl. J. Med.* **318**, 393 (1988).
- [14] H. Bruss, *Theoretical Microfluidics*, Oxford Master Series in Condensed Matter Physics (Oxford University, New York, 2008).
- [15] K. S. Suslick, *Science* **247**, 1439 (1990).
- [16] Y. T. Didenko, W. B. McNamara, and K. S. Suslick, *Phys. Rev. Lett.* **84**, 777 (2000).
- [17] H. Estrada, P. Candelas, A. Uris, F. Belmar, F. J. García de Abajo, and F. Meseguer, *Phys. Rev. Lett.* **101**, 084302 (2008).
- [18] B. Hou, J. Mei, M. Ke, W. Wen, Z. Liu, J. Shi, and P. Sheng, *Phys. Rev. B* **76**, 054303 (2007).
- [19] J. Christensen, L. Martín-Moreno, and F. J. Garcia-Vidal, *Phys. Rev. Lett.* **101**, 014301 (2008).
- [20] H. Estrada, F. J. García de Abajo, P. Candelas, A. Uris, F. Belmar, and F. Meseguer, *Phys. Rev. Lett.* **102**, 144301 (2009).
- [21] See Supplemental Material at <http://link.aps.org/supplemental/10.1103/PhysRevLett.108.124301> for more details on the theory.
- [22] S. Yang, J. H. Page, Z. Liu, M. L. Cowan, C. T. Chan, and P. Sheng, *Phys. Rev. Lett.* **93**, 024301 (2004).
- [23] J. Christensen and F. J. García de Abajo, *Appl. Phys. Lett.* **97**, 164103 (2010).